Electronic Supplementary Information

Rechargeable organic-air redox flow batteries

P. Leung[a], D. Aili[b], Q. Xu[c], A. Rodchanarowan[d], A. Shah[d,†]

a) Department of Materials, University of Oxford, Oxford, OX1 3PH, UK.

b) Department of Energy Conversion & Storage, Technical University of Denmark, Lyngby, Denmark.

c) School of Energy and Power Engineering, Jiangsu University, Zhenjiang 212013, China.

d) Department of Materials Engineering, Faculty of Engineering, Kasetsart University, 50 Ngamwongwan Rd., Ladyao, Chatuchak, Bangkok, 10900, Thailand

e) School of Engineering, University of Warwick, Coventry CV4 7AL, United Kingdom

† Author for correspondence. Email: Akeel.Shah@warwick.ac.uk

Experimental

Chemicals

3,3′-diaminobenzidine (DAB, ≥98%) was acquired from Glentham Life Sciences and stored at -18 °C. Isophthalic acid (IPA, 99%), polyphosphoric acid (PPA, 115% PA, reagent grade) and *N*,*N*-dimethylacetamide (DMAc) were supplied from Sigma Aldrich (Germany). Analytical grade quinoxaline and sodium hydroxide were supplied from Sigma Aldrich (Germany) and AKos GmbH (Germany). Solutions were prepared with distilled water or ultra-pure water (18 MΩ cm resistivity) from a Millipore water purification system (Milli-Q Integral 3). Typical electrolytes contain 0.050 M quinoxaline and 2 M sodium hydroxide for both cyclic voltammetry and charge-discharge experiments.

Preparation of the *m*-PBI separators

The poly(2,2′-(*m*-phenylene)-5,5′-bibenzimidazole) (*m*-PBI) was prepared through polymerization from IPA and DAB in stoichiometric amounts using poly(phosphoric acid) as polycondensation solvent, as described in more detail elsewhere [S1]. The inherent viscosity of the resulting *m*-PBI was 0.95 dL g^{-1} (500 mg dL^{-1} in 96% H_2SO_4 at 30.0 °C). The membranes were obtained by casting from DMAc on glass dishes at up to 120 °C, followed by treatment in boiling demineralized water for 2 h.

By submerging the resulting *m*-PBI in concentrated sodium hydroxide solutions (i.e. 10 M), a dynamic equilibrium between the pristine form of the membrane and the deprotonated ionic form. Such equilibrium depends on the concentration of the aqueous hydroxide solution, which shifts to the right when the concentration was increased. The preparation method and physiochemical properties of this membrane, i.e. volume change and chemical stabilities, have been evaluated by one of us in recent studies [S2].

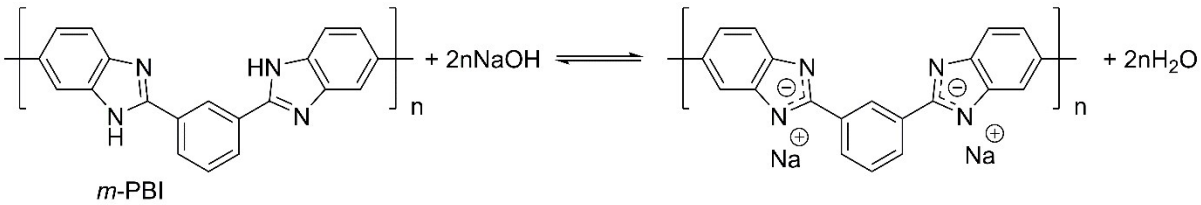

Scheme S1. Formation of sodium polybenzimidazolide repeating unit through deprotonation.

Area resistance of the *m*-PBI membrane

The area resistance of the hydroxide doped *m*-PBI membrane was measured in an in-house divided 'H-cell' with two electrolyte compartments, in which 2 M sodium hydroxide was filled as illustrated in Figure S1. The exposed area of the membrane was 2.5 cm × 2.5 cm, while the two graphite electrodes were placed at a distance of 2 cm from each other as an inter-electrode gap. The ionic resistances of the conductivity cell with and without membrane, were determined by the real axis intercept of the Nyquist plot using electrochemical impedance spectroscopy (Bio-logic VMP potentiostat (Bio-logic SAS, France) at frequency range from 1 MHz to 1 Hz with a 10 mV amplitude. The area resistance, *r*, was obtained from the follow equation:

$$r = (r_{\text{with membrane}} - r_{\text{without membrane}}) \times S$$

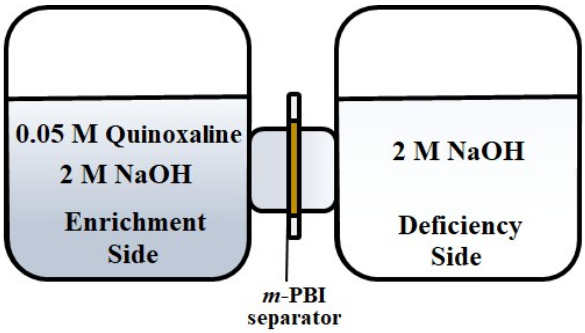

Figure S1. Schematics of 'H-cell' using for area resistance and permeability tests.

Permeability of quinoxaline across the *m*-PBI membrane

The permeability of quinoxaline across the membrane was evaluated using the same 'H-cell' as described for the measurement of the area resistance of the alkaline doped PBI membrane. One compartments was filled with 25 mL 50 mM quioxaline in 2 M sodium hydroxide, while the other compartment was filled only with 25 mL 2 M sodium hydroxide solution. At a regular time interval, samples in the deficiency side were taken and analyzed for the mass measurements. The permeability of quinoxaline was determined by:

$$V_D \frac{dc_d(t)}{dt} = A \frac{P}{L} (C_E - C_D(t))$$

where P is the permeability of the quinoxaline ($m^2\ s^{-1}$), V_D is the volume of the deficiency side (m^3), A is the effective area of the *m*-PBI membrane (m^2), L is the thickness of the membrane (m), C_E and C_D are the quinoxaline concentrations (mol dm^{-3}) in the enrichment and deficiency sides, respectively. It is assumed that the volumes of the electrolytes in the both sides were constant and the change in quinoxaline concentration in the enrichment side was negligible. This equation can be rearranged to the following equations:

$$\frac{dC_D(t)}{C_E - C_D(t)} = A\frac{P}{V_D L}dt$$

$$-\int_0^{C_D}\frac{d(C_E - C_D(t))}{C_E - C_D(t)} = A\frac{P}{V_D L}\int_0^t dt$$

Eventually,

$$\ln\left(\frac{C_E}{C_E - C_D}\right) = A\frac{P}{V_D L}t$$

The permeability of quinoxaline across the separators can be calculated by plotting the change in quinoxaline concentration as a form of $\ln\left(\frac{C_E}{C_E - C_D}\right)$ *vs*. time, where the gradient of the linear relationship corresponds to the values of $\frac{P}{V_D L}$.

Cyclic voltammetry & electrochemical impedance spectroscopy

A three-electrode acrylic glass cell with approximately 20 mL electrolyte was used for the cyclic voltammetry experiment, in which the working electrodes were either planar nickel, glassy carbon or manganese oxide 'air-breathing' electrodes. In addition to 'air-breathing' electrodes, the other two working electrodes were immersed in the electrolytes as in Figure S2. Counter and reference electrodes were carbon felt and mercury-mercuric oxide electrode (Bio-logic SAS., France). Cyclic voltammetry measurements were made using a Bio-logic VMP potentiostat (Bio-logic SAS, France) at a potential sweep rate in the range from 4 to 64 mV s^{-1}.

Unlike the cyclic voltammetry experiment, electrochemical impedance spectroscopy were taken in a flow battery rather than a three-electrode acrylic glass cell. Measurements were made by the same potentiostat in a potentiostatic mode with applied voltage amplitude of 10 mV at the open circuit voltage. The frequency range was between 100 kHz and 1 MHz, which took up to 5 min to finish each measurement. Electrolyte for negative half-cell measurement was 0.050 M quinoxaline and 2 M sodium hydroxide, while the electrolyte for the positive half-cell was 2 M sodium hydroxide.

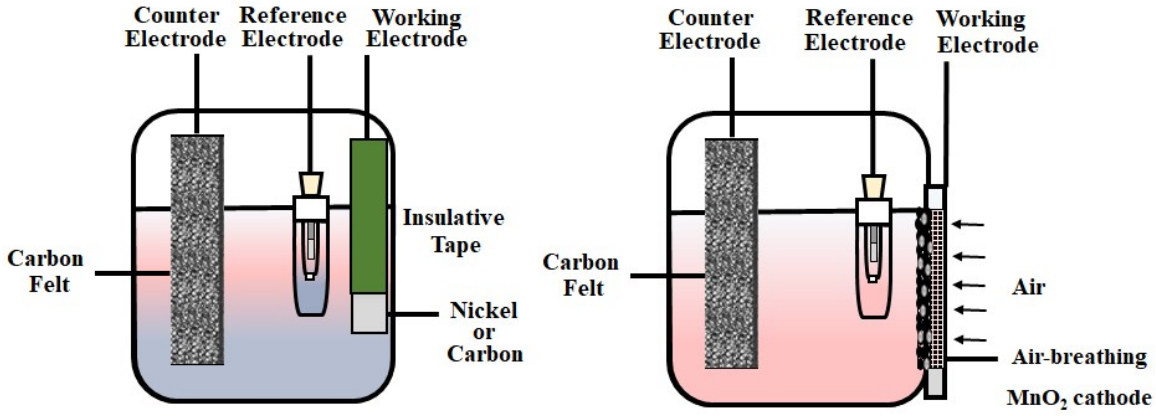

Figure S2. Schematics of experimental set-up for cyclic voltammetry experiments (glassy carbon was used for the negative half-cell measurements; planar nickel and air-manganese manganese dioxide were used for positive half-cell measurements.

Half- or full-cell galvanostatic charge-discharge cycling

The reduction and oxidation reactions of each half-cell reaction was carried out in a divided parallel plate flow cell, which is identical as the full-cell set-up. A prepared poly(2,20-(mphenylene)-5,50 -bibenzimidazole) (*m*-PBI) of 20 µm was used to separate the two compartments. As shown in Figure S3, the negative and positive half-cell compartments were composed of one (carbon felt, SGL Carbon GmbH, Germany) and two positive electrodes (pure nickel mesh, Goodfellow Inc., UK and manganese oxide based, E4, Electric Fuel Inc., Israel) , respectively. Each electrode had an active area of 2.5 cm × 2.5 cm (6.25 cm^2) with an inter-electrode gap of about 8 – 8.5 mm.

The negative electrolyte was 0.050 M quinoxaline and 2 M sodium hydroxide, while the positive electrolyte was 2 M sodium hydroxide. The volume of each electrolyte contained in separate tanks was 25 mL. Both electrolytes were circulated through the cell at a mean linear flow velocity between 0.34 and 0.90 $cm^3\ s^{-1}$. To minimize the oxidation of the reduced (negative) species, a fast stream of inert gas (nitrogen or argon) was purged in the negative electrolyte.

Reference electrode was placed at the entrance of each channel, in line with the electrolyte circuit. In a typical charge-discharge cycling experiment, negative and positive current densities of 7.5 mA cm^{-2} (46.9 mA) were applied and controlled by the working electrodes and the cell terminal for half-cell and full-cell measurements, respectively. Prior to half- or full-cell measurements, the electrolytes have been charge-discharge cycled for a few times. The electrical connections for the measurements of the half-cell electrode potentials ($E_{\text{quinoxaline}}$ and E_{air}), the overall cell voltages (E_{Cell}) and the ohmic drop of the electrolyte and membrane resistances between the two reference electrodes ($E_{\Delta\text{IR membr. \& electrolyte}}$) are clearly shown in Figure S3.

The coulombic, voltage and energy efficiencies were obtained as follows:

$$\text{Coulombic efficiency} = \frac{I_{discharge}\, t_{discharge}}{I_{charge}\, t_{charge}} \times 100\ \%$$

$$\text{Voltage efficiency} = \frac{V_{discharge}}{V_{charge}} \times 100\ \%$$

$$\text{Energy efficiency} = \frac{I_{discharge}\, V_{discharge}\, t_{discharge}}{I_{charge}\, V_{charge}\, t_{charge}} \times 100\ \%$$

where I is the applied current, V is the cell voltage and t is the duration of the process.

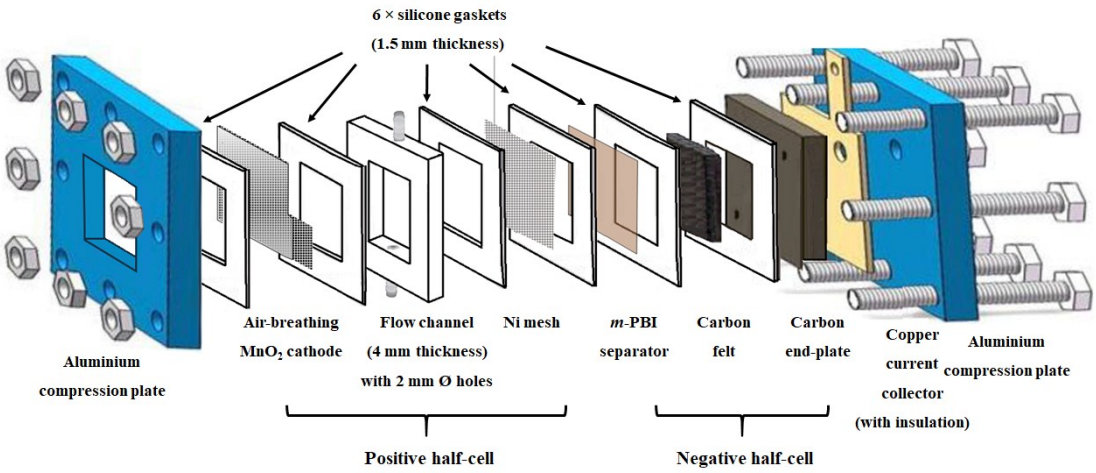

Figure S3. Experimental set-ups and components of the proposed organic-air redox flow batteries.

Alternative routes for quinoxaline reactions in alkaline electrolytes (pH > 7)

Alternative route:

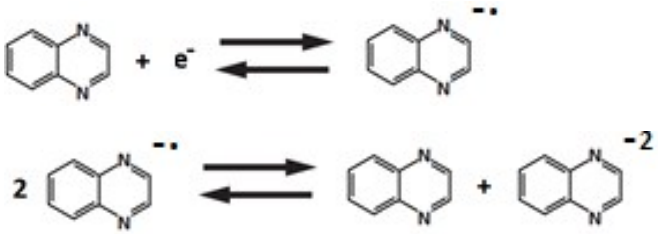

Standard electrode potentials in acidic electrolytes

Negative electrode reaction at < pH 7:

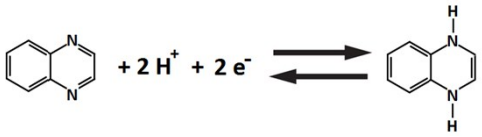

E= –0.66 V vs. SHE (1 M KCl, pH5.4) [21]

Positive electrode reaction at < pH 7:

$2\ H_2O \leftrightarrow O_2 + 4\ H^+ + 4\ e^-$ E= +1.23V vs. SHE (in acid, pH 0) [19]

Randles-Sevcik plots based on the reduction current density of quinoxaline

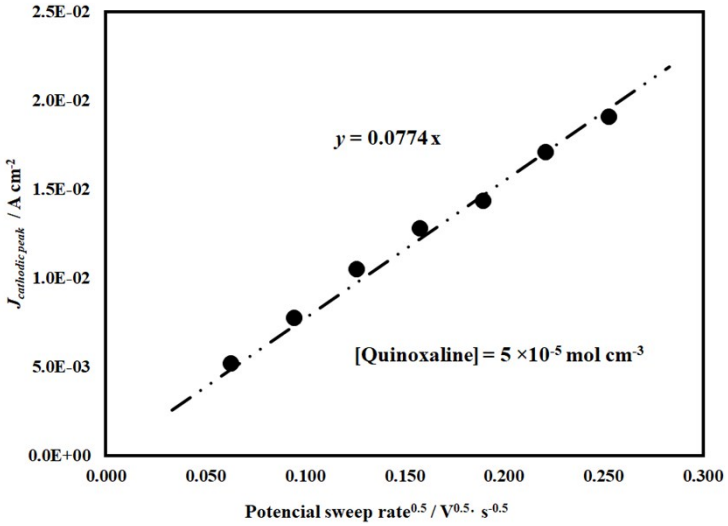

Figure S4. Randles-Sevcik plot based on the reduction current density of quinoxaline. The potential sweep rates were 4, 9, 25, 36, 49, 64 mV s^{-1} using glassy carbon electrodes.

Effect of quinoxaline concentrations in 0.2 M NaOH (less concentrated electrolytes)

Figure S5 shows the effect of the active material concentrations on the cyclic voltammetry of quinoxaline using a glassy carbon electrode at 10 mV s^{-1}. It is important to note that less concentration of sodium hydroxide (0.2 M) was used rather than 2 M as in the main text, which allow higher solubilities of quinoxaline (i.e. > 0.5 M). It can be seen that the cathodic current densities increase with the quinoxaline concentration until 0.45 M was reached. However, each increment was also found to be smaller, implying less effective reduction processes at higher quinoxaline concentrations.

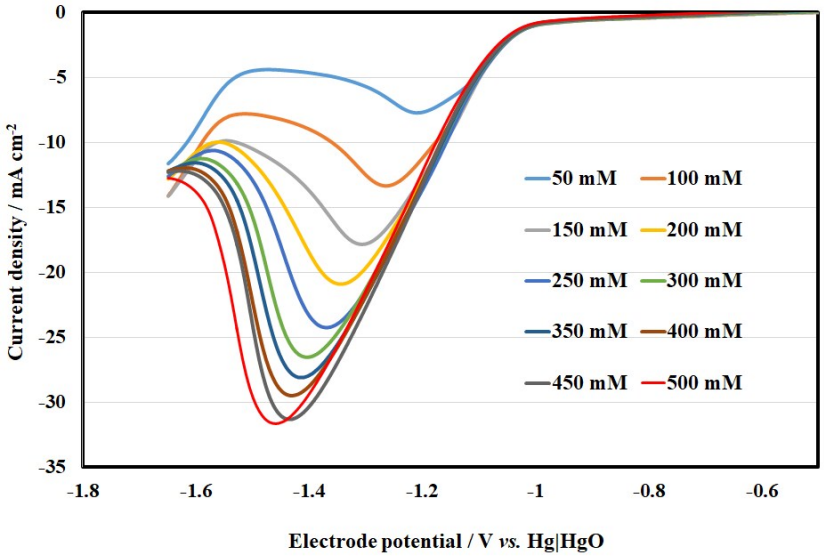

Figure S5. The effect of active material concentration on the reduction of quinoxaline in 0.2 M sodium hydroxide using glassy carbon electrode at 10 mV s^{-1}. Quinoxaline concentrations were 50, 100, 150, 200, 250, 300, 350, 400, 450, 500 mM.

Prolonged oxidation of 'air-breathing' manganese dioxide electrode

Figure S6 shows that electrode particles of the 'air-breathing' manganese dioxide based electrodes were observed to come off after 10 h of oxidation at 7.5 mA cm^{-2}, which resulted in a weight loss of up to 26 %. It shall be noted that the micrographs were taken after removing the insulative layers from the received electrodes.

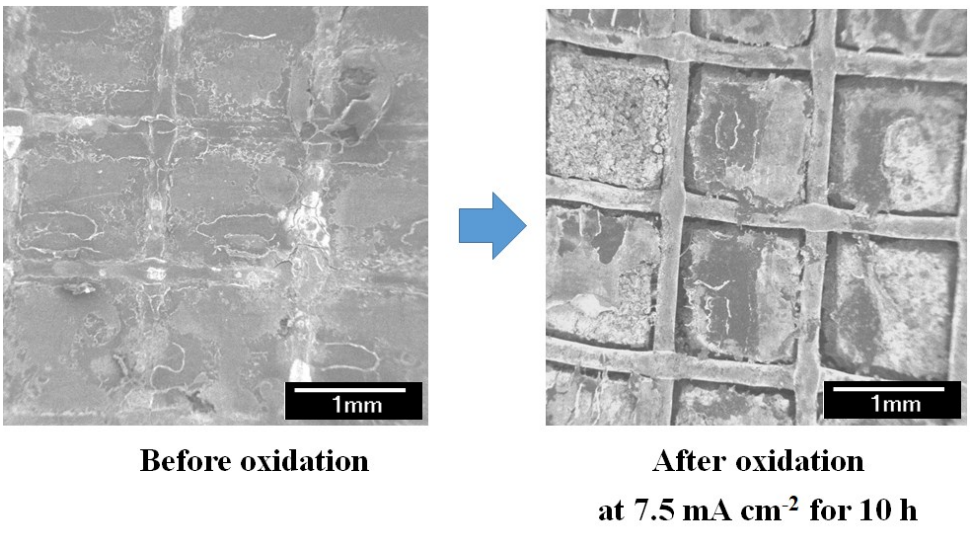

Figure S6. Scanning Electron Micrographs of 'air-breathing' manganese dioxide based electrodes before and after oxidation at 7.5 mA cm^{-2} for 10 h (magnifications: × 15).

Electrochemical impedance data fittings of half-cell/ full-battery reactions

	R_0	R_{int}	$R_{c.t.}$
Quinoxaline (carbon felt)	2.3	0.35	0.35
Air (air-breathing MnO_2)	5.4	0.7	0.8
Full-cell	18.1	1.9	2.3

Table S1. Calculated equivalent circuit resistance values calculated from electrochemical impedance data fitting to the equivalent circuit provided in Figure 5.

Quoted Cost and molecular weight of the active materials and supporting electrolytes

Elements	Cost	Molecular weight	Capacity in 1 Kg
Vanadium	USD$ 23.6 kg^{-1} [S3]	50.94 g mol^{-1}	526 Ah (1 e^-)
Sulfuric acid	USD$ 0.3 kg^{-1} [S4]	98.08 g mol^{-1}	N.A.
Quinoxaline	USD$ 2 kg^{-1} [S5]	130.2 g mol^{-1}	411 Ah (2 e^-)
Sodium hydroxide	USD$ 0.4 kg^{-1} [S6]	40.0 g mol^{-1}	N.A.

Electrolyte cost based on active materials per 1 kWh (theoretical capacity)

Chemistry	Energy	Discharge voltage	Required capacity	Weight of active materials	Cost of active materials (Theoretical capacity)
All-vanadium	1000 Wh	1.30 V	769 Ah	1.46 kg V + 1.46 kg V	USD$ 68.9
Quinoxaline-air	1000 Wh	0.7 V	1429 Ah	3.47 kg Quinoxaline	USD$ 5.2

Cost and energy density of various flow battery electrolytes

Flow battery systems	Cell voltage (open-circuit) / V	Negative species cost (element)$^{+}$ / USD$ Kg^{-1}	Positive species cost (element)$^{+}$ / USD$ Kg^{-1}	Electrolyte cost* / USD$ (kW h)$^{-1}$	Typical energy density / W h L^{-1} [s7]
Zn-Fe	1.5	1.9	0.8	5	-
Zn-Ce	2.4	1.9	12	42	12 – 20
Zn-I	1.3	1.9	13.5	41	Up to 101
Zn-Organic (Benzoquinone)	1.6	1.9	3	10	2 – 5
Zn-air	1.6	1.9	N.A.	4	-
Zn-Br	1.8	1.9	2	5	Up to 65
V-V	1.4	24	24	87	15 - 43
All-Organic (Viologen-TEMPO)	1.2	3 – 5 (est.)	3 – 5 (est.)	55 – 92	0.5 – 5
Quinoxaline-air	0.9	2 [s4]	N.A.	32 (this work , 16 % capacity is used) 16 (projected if 32 % capacity is used) 10 (projected if 50 % capacity is used)	1.1 (this work, 0.05 M quinoxaline, 16 % capacity is used) 22 (projected if 1 M quinoxaline, 16 % capacity is used or if 0.5 M quinoxaline, 32 % capacity is used)

+ Element costs are from the latest USGS Materials Databook

* Estimated by assuming 80 % voltage efficiencies for zinc-based flow batteries; 90 % voltage efficiency for all-vanadium redox flow batteries; 50 % electrolyte utilization for electrodeposition reaction; 80 % electrolyte utilization for liquid-phase redox reaction.

Component costs of redox flow battery module:

Components	Cost	References
Bipolar plate, USD$ m^{-2}	55	[S8]
Graphite felt, USD$ m^{-2}	70	[S8]
Nickel mesh, USD$ m^{-2}	15	[S9]
Manganese dioxide (electrode grade), USD$ m^{-2} (assuming 1 kg is for 1 m^2; USD$0.5 kg^{-1})	0.5	[S10]
Stainless steel mesh for air cathode, USD$ m^{-2}	12	[S11]

PVC frame, USD$ m^{-2}	16.56	[S8]
Nafion® Membrane, USD$ m^{-2}	220	[S12]
Celazole® PBI Membrane, USD$ m^{-2} (20 μm; 38.5 m^2 kg^{-1}; 1.3 g cm^{-3}; USD$1350 kg^{-1} [S13])	35	Calculated
Gaskets, bolts, end-plate, USD$ m^{-2}	14	[S8]
Pump, per item, USD$ (2 pumps per stack)	178	[S14]
Battery management system, per item, USD$ (1 battery management system per stack)	550	[S14]
Vanadium, USD$ kg^{-1}	23.6	[S3]
Quinoxaline, USD$ kg^{-1}	2	[S5]

Cost estimations of redox flow battery module

Dimensions of a 100-cells stack based on Regenesys® module

Dimension of each 100-cells stack: 155 cm × 150 cm × 80 cm **(see Figure S10a)**

Inter-electrode gap: 0.75 cm **(see Figure S10b)**

Electrode area: 108 cm × 67 cm = 7236 cm^2 or 0.723 m^2 **(see Figure S10c)**

PVC frame area: 108 cm × 67 cm = 7236 cm^2 or 0.723 m^2 **(see Figure S10c)**

Membrane area (assumed): 110 cm × 70 cm = 7700 cm^2 or 0.77 m^2 **(see Figure S10c)**

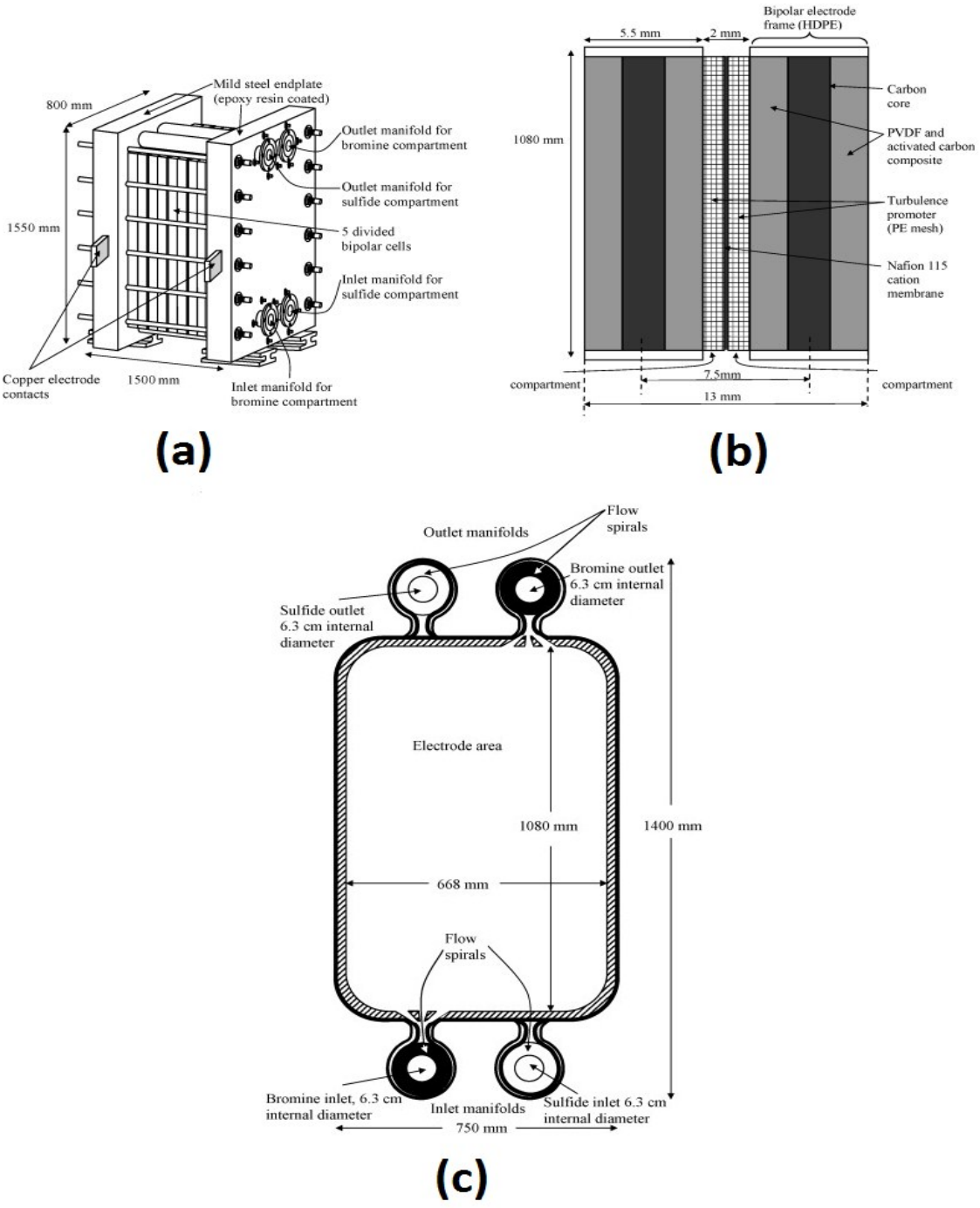

Figure S7. (a) Lateral view of the Regenesys® module showing the inlet and outlet manifolds and the location of the current collectors. Not to scale. (b) Details of a bipolar cell showing the main components. Not to scale. The dimensions are nominal. (c) Electrode configuration showing the location of the spirals and the projected electrode area [S15].

Estimated cost of a Regenesys® module for all-vanadium chemistry

(a) Cost of bipolar plate

= 0.723 m^2 × 101 items ×USD$ 55 m^{-2}

= USD$ 4016.3

(b) Cost of graphite felts

= 0.723 m^2 × 200 items ×USD$ 70 m^{-2}

= USD$ 10122

(c) Cost of PVC frame

= 0.723 m^2 × 101 items ×USD$ 16.6 m^{-2}

= USD$ 1212.2

(d) Cost of Nafion membrane

= 0.77 m^2 × 100 items ×USD$ 220 m^{-2}

= USD$ 16940

(e) Cost of gaskets, bolts and end-plates

= 0.723 m^2 × 200 items ×USD$ 14 m^{-2}

= USD$ 2024.4

(f) Cost of pumps

= 2 items × USD$ 178

= USD$ 356

(g) Cost of battery management systems

= 1 item × USD$ 550

= USD$ 550

Estimated cost of a Regenesys® module for quinoxaline-air chemistry

(a) Cost of bipolar plate

= 0.723 m^2 × 101 items ×USD$ 55 m^{-2}

= USD$ 4016.3

(b) Cost of graphite felts

= 0.723 m^2 × 100 items ×USD$ 70 m^{-2}

= USD$ 5061

(c) Cost of nickel mesh electrode

= 0.723 m^2 × 100 items ×USD$ 15 m^{-2}

= USD$ 1084.5

(d) Cost of manganese dioxide electrode

= 0.723 m^2 × 100 items ×USD$ 0.5 m^{-2}

= USD$ 36.2

(e) Cost of stainless steel mesh for air cathode

= 0.723 m^2 × 100 items ×USD$ 12 m^{-2}

= USD$ 867.6

(f) Cost of PVC frame

= 0.723 m^2 × 101 items ×USD$ 16.6 m^{-2}

= USD$ 1212.2

(g) Cost of PBI membrane

= 0.77 m^2 × 100 items ×USD$ 35 m^{-2}

= USD$ 2695

(h) Cost of gaskets, bolts and end-plates

= 0.723 m^2 × 200 items ×USD$ 14 m^{-2}

= USD$ 2024.4

(i) Cost of pumps

= 2 items × USD$ 178

= USD$ 356

(j) Cost of battery management systems

= 1 item × USD$ 550

= USD$ 550

Total estimated cost of a Regenesys® module

Cell components	All-vanadium		Quinoxaline-air	
	Cost / USD$	Percentage/ %	Cost / USD$	Percentage/ %
Electrodes	14138.3	40.1	11065.6	61.8
PVC frame	1212.2	3.4	1212.2	6.8
Membrane	21560	48.1	2695	15.1
Gaskets, bolts and end-plate	2024.4	5.7	2024.4	11.3
Pumps	356	1.0	356	2.0
Battery management system	550	1.6	550	3.1
Total	**35220**	**100**	**17903**	**100**

References

[S1] A. Kirkebaek, D. Aili, D. Henkensmeier, J.O. Jensen, Q. Li, Gel Electrolytes of Covalent Network Polybenzimidazole and Phosphoric Acid by Direct Casting, Macromol. Mater. Eng, 2017, 302, 1700347.

[S2] D. Aili, A. Jankova, J. Han, N.J. Bjerrum, J. O. Jensen, Q. Li, Understanding ternary poly(potassium benzimidazolide)-based polymer electrolyte, *Polymer*, 2016, 84, 304 – 310.

[S3] http://mineralprices.com/

[S4] https://www.alibaba.com/product-detail/98-Industrial-Grade-Sulphuric-Acid-H2SO4_60655020087.html?spm=a2700.7724838.2017115.16.3fbad2436jgzba

[S5] https://www.alibaba.com/product-detail/Quinoxaline-CAS-NO-91-19-0_1508423411.html?spm=a2700.7724838.2017115.286.3ce736b51rKO4w

[S6] https://www.alibaba.com/product-detail/ISO-BV-certificated-for-detergent-and_60583424290.html?spm=a2700.7724838.2017115.19.3fbad2436jgzba&s=p

[S7] G.M. Weng, Z. Li, G. Cong, Y. Zhou, Y.C. Lu, 'Unlocking the capacity of iodide for high-energy-density zinc/polyiodide and lithium/polyiodide redox flow batteries', Energy & Environ. Sci., 3 (2017) 735-741.

[S8] Y.K. Zeng, T.S. Zhao, L. An, X.L. Zhou, L. Wei, A comparative study of all-vanadium and iron-chromium redox flow batteries for large-scale energy storage, J. Power Sources,

2015, 300, 438 – 443.

[S9] https://www.alibaba.com/product-detail/High-quality-Pure-nickel-woven-wire_60277904954.html?spm=a2700.7724838.2017115.64.3ce736b51rKO4w

[S10] https://www.alibaba.com/product-detail/electrodes-manganese-dioxide_60572683416.html?spm=a2700.7724838.2017115.26.3ce736b51rKO4w

[S11] https://www.alibaba.com/product-detail/304-316-20Mesh-Plain-Woven-Stainless_60181242736.html?spm=a2700.7724838.2017115.155.2cd56063lkvYKI

[S12] https://www.alibaba.com/product-detail/Perfluorinated-ion-exchange-membrane-PEM-membrane_60640300737.html?spm=a2700.7724838.2017115.31.23369882UzTza4

[S13] https://www.alibaba.com/product-detail/CELAZOLE-PBI-small-plate_60410118580.html?spm=a2700.7724838.2017115.194.62257e50c6fxZY

[S14] L. Joerissen, J. Garche, Ch. Fabjan, G. Tomazic, Possible use of vanadium redox-flow batteries for energy storage in small grids and stand-alone photovoltaic systems, J. Power Sources, 127, 2004, 98 -104.

[S15] C. Ponce de Leon, G.W. Reade, I. Whyte, S.E. Male, F.C. Walsh, Characterization of the reaction environment in a filter-press redox flow reactor, Electrochim. Acta, 2007, 52, 5815 – 5823.